Experimental and Theoretical Studies on the Complexes of $[Pb_m-Pyridyl]^-$ ($m = 1-4$)

Xiao-Jing Liu,[†] Ke-Li Han,*[,†] Shu-Tao Sun,[‡] Zi-Chao Tang,*[,†] Zheng-Bo Qin,[§] and Zhi-Feng Cui[§]

State Key Laboratory of Molecular Reaction Dynamics, Dalian Institute of Chemical Physics, Chinese Academy of Sciences, Dalian 11602, P. R. China, State Key Laboratory of Molecular Reaction Dynamics, Center of Molecular Science, Institute of Chemistry, Chinese Academy of Sciences, Beijing 100080, P.R. China, and Department of Physics, Anhui Normal University, Wuhu, Anhui Province 241000, P.R. China

Received: December 4, 2007; Revised Manuscript Received: April 24, 2008

The pyridyl−lead complexes $[Pb_m-C_5H_4N]^-$ ($m = 1-4$), which are produced from the reactions between lead clusters formed by laser ablation and the pyridine molecules seeded in argon carrier gas, are studied by photoelectron (PE) spectra and density functional theory. The adiabatic electron affinity (EA) of $[Pb_mC_5H_4N]^-$ is obtained from PE spectra at photon energies of 308 and 193 nm. Theoretical calculation is carried out to elucidate their structures and bonding modes. A variety of geometries for the isomers are optimized to search for the lowest-energy geometry. By comparing the theoretical results, including the EA and simulated density of state spectra, with the experimental determination, the lowest-energy structures for each species are obtained. The following analysis of the molecular orbital composition provides the evidence that the pyridyl binds on lead clusters through the Pb−C σ bond. Moreover, there is an apparent spin-state transition from triplet state toward singlet state for the ground-state structure of $[Pb_mC_5H_4N]^-$ with an increase of lead cluster.

1. Introduction

The adsorption of molecule or fragment on metal surface is an important field in surface science.[1–3] Verifying the structure and property of the adsorbate on the metal can develop a microscopic level description of heterogeneous catalysis, organometallic reactions in condensed phase, and electron transfer involved in biological systems.[4–10] Because the active site in the catalytic reaction is localized near the edge or the defect of metal surface, studying of the fragment adsorbed on small metal clusters can be a promising platform for catalysis and nanoassembly. The recent report that the steric effect strongly influences the adsorption of molecule onto the metal surface clarifies the dynamics in the entrance channels of the potential energy surfaces controlling the catalytic process.[11] It is recognized that the cluster science not only can elucidate the properties of condensed phase but also can provide detailed information on the reaction mechanisms and the nature of the reaction sites that enable certain catalytic substance to be especially effective.

Metal complexes of N-donor heterocyclic ligands are very important in biological systems, environmental issues, electrochemical applications, and supramolecular chemistry.[12–16] The heavy metal ions play active roles in a variety of biological processes, being components of proteins, nucleic acids, vitamins, and drugs.[17] In all of these examples, the interactions between the metal ion and *N*-donor ligands play a critical role in the biochemical processes that occur in organisms. For example, pyridine (C_5H_5N), an azabenzene, is an aromatic molecule consisting of a π-electron ring and a nitrogen atom. It is one of the most abundant and best known of the aromatic heterocyclic compounds widely distributed in nature, principally as enzymes and alkaloids. Pyridine is also used as a building block of many pharmaceuticals with different functionalities.[17]

Recently, the adsorption of pyridine on the surface of metal has been studied extensively. Tian and co-workers have studied the Raman spectra of pyridine adsorbed on the metal surface of Fe, Co, Ni, Cu, Ag, Au, Ru, Rh, and Pt, which indicate that it is chemisorption and the pyridine is perpendicular or declining on the surface of the metal through the end of the N atom.[18–24] Rodger and co-workers have found the periodic trends in the binding of metal cations (Mg^+, Al^+, Sc^+, Ti^+, V^+, Cr^+, Mn^+, Fe^+, Co^+ Ni^+, Cu^+, and Zn^+) to pyridine by threshold collision-induced dissociation and density functional theory (DFT).[25] The bonding energies of metal-cation−pyridine complexes containing Cu, Ag, and Au have been confirmed by photodissociative experimental and theoretical studies.[26,27] However, these studies are just focused on the transition metal species, and much work is still required on the reactions of the main group metals.

Lead has an electronic structure completely different from those of the transition metals, and many unfilled orbitals or unpaired electrons (for example, those in Pb_m^-) are presented in lead clusters. This may exert an effect on their reactions or bonds with pyridine. In industry, lead is involved in some important catalytic processes. Lead ruthenate has a catalytic activity comparable to that of platinum in the catalytic decomposition of hydrogen peroxide in alkaline solutions.[28] Lead halides are used to catalyze the allylation of biphenyl ether with allyl bromide and give good functional selectivity.[29] In addition to its practical applications, the study of ionic lead clusters is also of fundamental interest. In 1972, Castleman and co-workers[30] studied the gas-phase hydration of the monovalent lead cation by using high-pressure mass spectrometry, and clusters of up to eight water molecules around a lead cation were observed. Later, they reported the combination reaction of benzene with lead cation, and Pb^+−benzene displayed an unusually strong interaction.[31] Stace and co-workers[32] found that lead cluster cations could combine with methanol molecule to

* Corresponding author. E-mail: klhan@dicp.ac.cn.
† Dalian Institute of Chemical Physics, Chinese Academy of Sciences.
‡ Institute of Chemistry, Chinese Academy of Sciences.
§ Anhui Normal University.

10.1021/jp711459x CCC: $40.75
Published on Web 07/10/2008

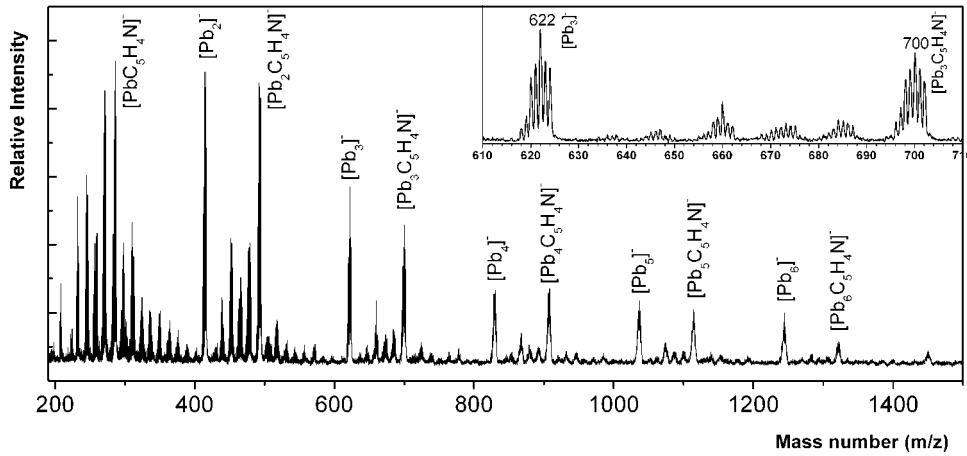

Figure 1. Typical mass spectra of the anion products by laser vaporization/ionization of lead samples into a mixture of argon and pyridine (C_5H_4N).

form lead−methanol complex, and the lead moiety can catalyze the bimolecular dehydration through the O−H insertion. In our previous publications,[33–36] the reactions of lead cluster ions with benzene, alkene, or acetone were reported, in which the C−C or C−H bond is inserted through high-energy reaction pathways. To the best of our knowledge, the interaction between the lead anion cluster and pyridine has not been reported.

The anion photoelectron (PE) spectra is a powerful experimental tool in probing the electronic structure of clusters.[37–40] In this paper, we report brand new anion complexes [Pb$_m$−C$_5$H$_4$N]$^-$ (m = 1−4) by mass spectrometry and anion PE spectroscopy, which are produced from reactions between pyridine and vapor lead generated by laser ablation on a lead solid sample. By a combination of experimental and theoretical studies, a significant understanding of bonding, geometric, electronic structure, and orbital composition of the [Pb$_m$−C$_5$H$_4$N] $^-$ (m = 1−4) are obtained. It is our hope that the reported results will aid in the deep study on physics and chemistry of lead-cluster complexes.

2. Experimental Methods

The apparatus used in the experiments mainly consists of a homemade reflectron time-of-flight mass spectrometer (RTOFMS) with high resolution and a PE spectrometer with a magnetic-bottle-type analyzer. Details of the apparatus have been published elsewhere.[41] Here, a brief description is presented. The lead disk targets (99.9%) in the source chamber of the RTOFMS are rotated and ablated by a pulsed laser beam (532 nm Nd:YAG laser, 10 Hz, 10 mJ/pulse). The laser-induced plasma is carried by a molecular beam generated by a pulsed valve at a backing pressure of about 400 kPa of argon (purity 99.99%), in which pyridine is seeded. The volume ratio of pyridine in the mixed gas is about 0.2%. The Pb$_m$−pyridyl cluster anion products from the reactions of lead and pyridine are entrained by the carrier gas and undergo low pressure (10^{-2} Pa) in the source chamber. After passing a skimmer, all products enter into the acceleration area in the spectroscopic chamber (10^{-4} Pa). The negatively charged clusters are accelerated in the direction perpendicular to the molecular beam and are reflected toward the detector, microchannel plates. The RTOFMS resolution ($M/\Delta M$) is better than 2000; therefore, it is easy to resolve the number of hydrogen atoms in the products. The products can be mass-selected by the timing probe. The anions are photodetached by a XeCl excimer laser (308 nm), and the detached PEs are measured by the PE spectrometry, a magnetic-bottle time-of-flight analyzer, calibrated by the known spectra of Ag$^-$ and Au$^-$. The energy resolution of the instrument is approximately 70 meV for 1 eV electrons.

3. Computational Methods

All the calculations are accomplished with Gaussian03 program.[42] All full optimizations of geometries and harmonic vibration frequency calculations are performed with the method of three-parameter hybrid functional of Becke by using the Lee−Yang−Parr correlation functional (B3LYP)[43] of DFT. The standard basis set 6-311G(d,p) is used for C, H, and N atoms. The LANL2DZdp[44] basis set is adopted for lead atoms, which includes the relativistic effective core potentials by using the double-ζ(DZ) basis sets augmented by a set of d-type polarization functions. The DZ basis set for the hydrogen element was augmented by a set of p-type polarization functions (p exponent 0.356). The d exponents used for Pb are 0.179. These theoretical methods have been used to study the structure and energy of organo-lead molecules or lead clusters extensively.[45–50] Because the energy difference between ^{1}[Pb$_2$C$_5$H$_4$N]$^-$ and ^{3}[Pb$_2$C$_5$H$_4$N]$^-$ is small, further calculation is performed with the larger basis set aug-cc-pvtz-pp [51,52] for Pb, called as 6-311++g**(C, H, N)/aug-cc-pvtz-pp(Pb). All energies reported here are corrected with the zero-point vibrational energy.

4. Results and Discussion

4.1. Mass Spectra and PE Spectra Study on [Pb$_m$(C$_5$H$_4$N)]$^-$ Complexes. As shown in Figures 1 and 2, anion pyridyl−lead complexes [Pb$_m$C$_5$H$_4$N]$^-$ and [Pb$_m$C$_5$D$_4$N]$^-$ are the dominant products of the reactions. The PE spectra of [Pb$_m$C$_5$H$_4$N]$^-$ (m = 1−4) at 308 nm are shown in Figure 3. The anions are supposed to be in their electronic ground state because they are cooled in supersonic expansion. Each of these PE spectra represents a transition from the ground state of the anions to the ground or excited electronic states of the neutrals. Because the photodetachment process is much faster than the movement of the nuclei, PE spectra provide the electronic and vibrational (if the resolution is sufficient) information of the neutral species corresponding to the anionic cluster geometry. Electron affinity (EA) is defined as the energy of the origin transition between the ground state of the anion and the ground state of the neutral. As can be seen in Figure 3, the position, indicated by the arrow, is evaluated to be the EA of the corresponding complex. The adiabatic EA values of [Pb$_m$C$_5$H$_4$N]$^-$ (m = 1−4) are listed in

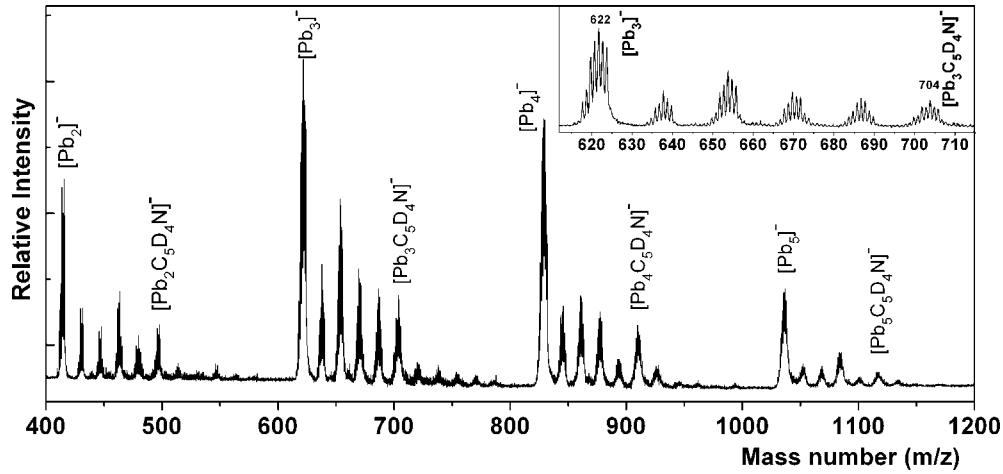

Figure 2. Typical mass spectra of the anion products by laser vaporization/ionization of lead samples into a mixture of argon and pyridine (C_5D_4N).

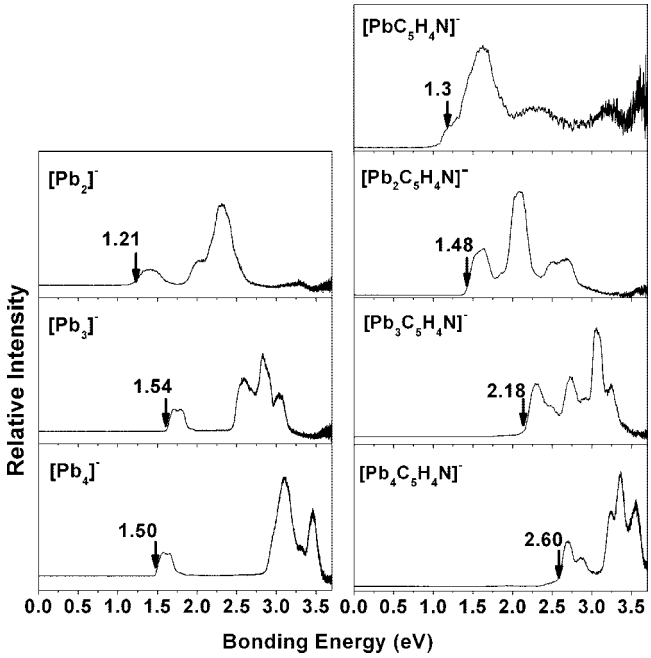

Figure 3. PE spectras of $[Pb_m]^-$ ($m = 1-3$) and $[Pb_mC_5H_4N]^-$ ($m = 1-4$) at 4.03 eV photon energy (308 nm).

TABLE 1: Various Structural and Energetic Characteristics for Neutral and Anionic Complexes of PbC_5H_4N

cluster	isomer	R_{Pb-C} (Å)	ΔE (eV)	EA (eV)
$[PbC_5H_4N]^-$	p-^{1}1a	2.370	0.83	0.57
	p-^{3}1a	2.340	0	1.40
	m-^{1}1a	2.357	0.85	0.52
	m-^{3}1a	2.349	0.08	1.29
	o-^{1}1a	2.236	0.89	0.32
	o-^{3}1a	2.337	0.32	0.89

Tables 1–4. The measured EA values of Pb_m^- ($m = 2-5$) and their spectra features are consistent with the results in refs 37, 53–55 within experimental error.

The electron detachment threshold, EA, of every $[Pb_mC_5H_4N]^-$ ($m = 1-4$) is comparatively higher than that of the corresponding naked lead clusters Pb_m^-.[35] After the bonding of Pb_m^- with the C_5H_4N group, the symmetries of the products are lowered, and the original degenerate orbitals (for example, $6p_x6p_y6p_z$ for Pb^-, $6p\pi$ for Pb_2^-, etc.) are transformed into nondegenerated ones. The MOs near the HOMO are rearranged

TABLE 2: Various Structural and Energetic Characteristics for Complexes of $[Pb_2C_5H_4N]^-$

cluster	isomer	R_{Pb-C} (Å)	ΔE (eV)	EA (eV)
$[Pb_2C_5H_4N]^-$	p-^{1}2a	2.445	0	1.80
	p-^{3}2a	2.405	0.19	1.61
	m-^{1}2a	2.466	0.04	1.74
	m-^{3}2a	2.399	0.22	1.56
	o-^{1}2a	2.427	0.28	1.08
	o-^{3}2a	2.381	0.42	0.94

and have a lower energy level with the contribution of the formed Pb−C bond. These facts enhance the electron detachment threshold. Further description of this result with the help of theoretical calculation can be seen in Sections 4.2 and 4.4. For the $[Pb_2C_5H_4N]^-$, the spectral features of the two peaks in $[Pb_2C_5H_4N]^-$ are clearly different; the first peak into the ground state is broad, whereas that second peak into the first excited state is sharp, which is attributed to a geometric change from the anion to the neutral. For $[Pb_mC_5H_4N]^-$ ($m = 1-4$), the PE spectra (including the EAs, the slow rising tails, and the first and the second electron peaks) are similar to that of $[Pb_mC_6H_5]^-$ ($m = 1-4$), in which the phenyl group provides a single electron to combine with Pb_m through Pb−C σ bond.[36] In addition, the PE spectra of $[Pb_4C_5H_4N]^-$ is also very similar to that of $[Pb_4F]^-$, in which the F atom surely combines with Pb_4 with a single chemical bond and has a closed-shell structure.[37] This implies that the pyridyl adsorb on the surface of the lead cluster through a single Pb−C σ bond in $[Pb_4C_5H_4N]^-$ with closed-shell electron state, which will be further explained by the following theoretical investigation.

4.2. Theoretical Low-Energy Structures. To interpret the experimental results, the structures of Pb_m^- ($m = 2-4$) and $[Pb_mC_5H_4N]^-$ ($m = 1-4$) are optimized by DFT method. Figure 4 presents the optimized stable structures of these complexes, and their structural and energetic characteristics are summarized in Tables 1–4. Because the Pb atom has a $6p^2$ electron configuration, two states including singlet and triplet are considered for the ground state of Pb_m and $[Pb_mC_5H_4N]^-$ ($m = 1-4$), whereas doublet and quartet states are considered for the ground state of Pb_m^- and $Pb_mC_5H_4N$. Because the ortho, meta, and para positions of the nitrogen atom in pyridine are not equivalent, we consider these three different kinds of substitute modes of lead clusters on pyridine.

The ground state of neutral Pb_m is found to be a singlet state, whereas that of anion Pb_m^- is a doublet state. Therein, the triangle geometry of ground-state Pb_3 or Pb_3^- is the lowest

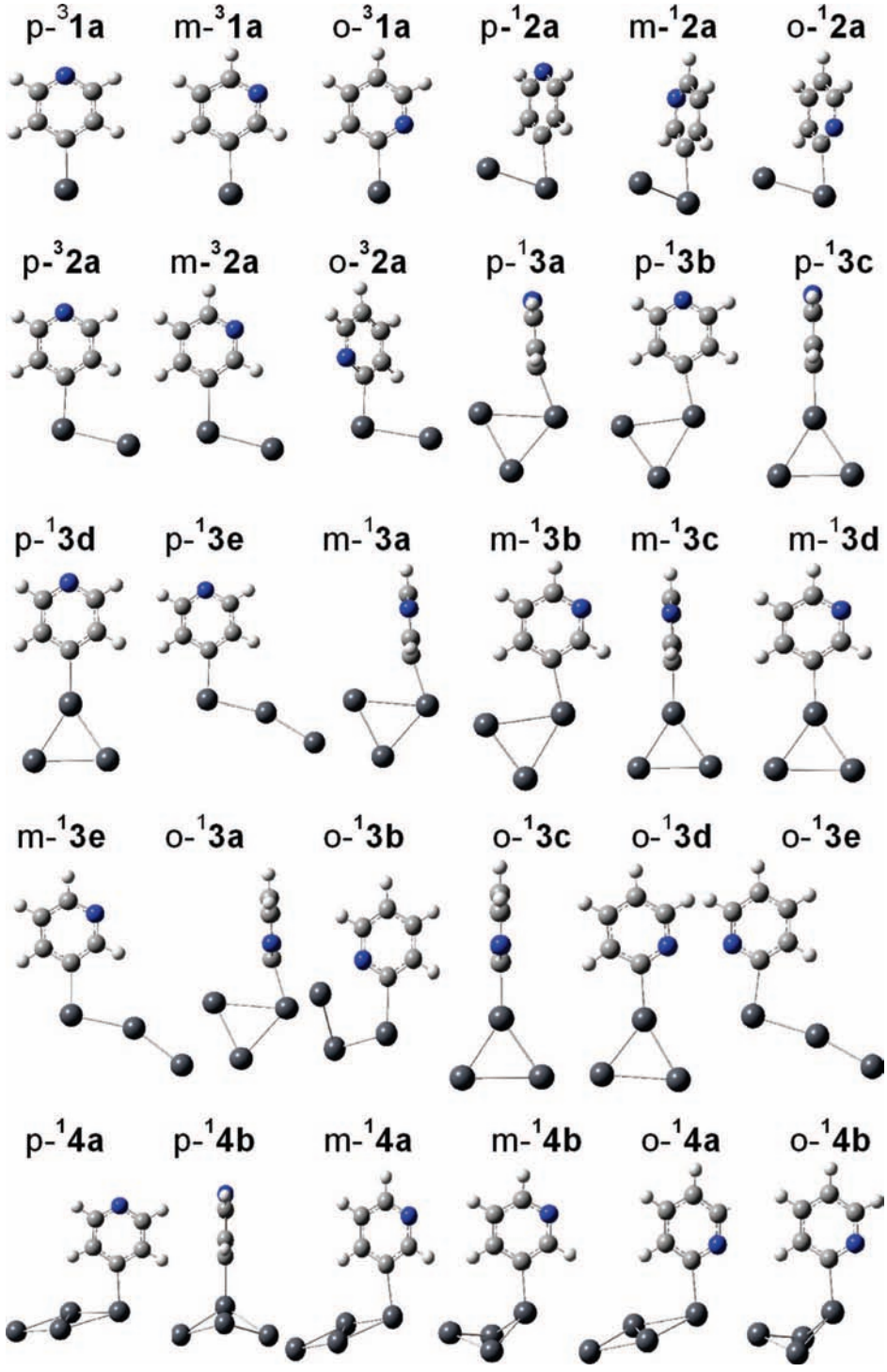

Figure 4. Optimized structures for anionic complexes of [Pb$_m$C$_5$H$_4$N]$^-$ (m= 1−4).

energy structure, whereas for the ground-state Pb_4 or Pb_4^-, the lowest-energy configuration is the rhombus geometry, which are all in accordance with the earlier studies.[37,53–55] All the Pb−Pb bond lengths of Pb_m^- obtained here are consistent with the earlier reported data.[37,53–55]

For both neutral and anion Pb$_m$C$_5$H$_4$N (m = 1−4), a variety of structures are considered. For all of the neutral Pb$_m$C$_5$H$_4$N (m = 1−4), the doublet-state configurations are much more stable than the quartet-state ones. There is a small difference of energy among the neutral (o, m, p)-Pb$_m$C$_5$H$_4$N with doublet state. However, for the anion [Pb$_m$C$_5$H$_4$N]$^-$ (m = 1−4), the (m, p)-[Pb$_m$C$_5$H$_4$N]$^-$ are more stable than the o- [Pb$_m$C$_5$H$_4$N]$^-$. Then, the o-[Pb$_m$C$_5$H$_4$N]$^-$ (m = 1−4) is not the preferable configuration in energy. Moreover, there exist an apparent spin-state transition from triplet state toward singlet state for the [Pb$_m$C$_5$H$_4$N]$^-$ with an increase of lead cluster. For the anion [PbC$_5$H$_4$N]$^-$, the triplet-state configuration is much more stable than the singlet-state one, in which the lead atom couples on the pyridyl through the coplanar Pb−C bond. For the anion [Pb$_2$C$_5$H$_4$N]$^-$, the singlet-state configuration has an energy a little bit more stable than that of the triplet state configuration. The energy difference between the singlet state and triplet state is only about 4 kcal/mol, which is in the range of coexisting energy of isomer. The pyridyl couples with the lead atom through the Pb−C bond, and the two lead atoms are nonplanar with the pyridyl in ^{1}[Pb$_2$C$_5$H$_4$N]$^-$, whereas the pyridyl are

coplanar with the lead atoms in neutral $^2[Pb_2C_5H_4N]$ and anion $^3[Pb_2C_5H_4N]^-$. As a result, the geometric change from the anion $^1[Pb_2C_5H_4N]^-$ to the neutral $^2[Pb_2C_5H_4N]$ leads to the first peak is broader than second one in experimental PE spectra. For the anion $[Pb_3C_5H_4N]^-$, the singlet-state configuration is much more stable than the triplet-state one. There are five low-energy isomeric structures *1*(**3a**−**e**) for the $^1[Pb_3C_5H_4N]^-$. Isomer ^{1}**3a** is the lowest-energy structure, where the pyridyl couples with the lead atom through the Pb−C bond and the face of Pb_3 group is perpendicular to the plane of the pyridyl. Isomer ^{1}**3b** is the nearest to ^{1}**3a** in energy, in which the Pb_3 group is coplanar with the pyridyl. The small energy difference between these two isomers implies that the pyridyl could rotate freely though C−Pb bond in $[Pb_3C_5H_4N]^-$, and this bonding mode should be a σ bond. The energies of isomers ^{1}(**3c**−**e**) are much higher than those of ^{1}**3a** and ^{1}**3b**. For the $[Pb_4C_5H_4N]^-$, the singlet-state configuration is also much more stable than the triplet-state one. There are two low-energy isomeric structures ^{1}(**4a**,**b**). Isomer ^{1}**4a** is the stable structure, in which the Pb_4 cluster has a rhombus configuration and couples with the pyridyl through Pb−C bond. Isomer ^{1}**4b** could be ruled out because of its much higher energy than that of ^{1}**4a**.

Obviously, it is easier for the open-shell Pb_m^- ($m = 2-4$) to lose an electron to form the closed-shell Pb_m than for the closed-shell $[Pb_mC_5H_4N]^-$ ($m = 2-4$) to lose an electron to form the open-shell $Pb_mC_5H_4N$, which results in the EA of $[Pb_mC_5H_4N]^-$ being larger than that of the corresponding Pb_m^-. The $[Pb_2C_5H_4N]^-$ has two coexisting spin state, including singlet and triplet states, which leads to the EA to be similar to that of Pb_2^-. This provides an excellent explanation for the experimental PE spectra findings.

4.3. Assignments of the Complex Structures. The assignment of the most possible structures of $Pb_mC_5H_4N$ is given on the basis of relative energy, EA, and the simulated density of state (DOS) spectrum. This structural assignment method has been widely used in cluster study.[56–56] The relative energy has been provided above. Now, the EAs of all complexes are calculated and are listed in Tables 1–4. The theoretical DOS is shifted by setting the HOMO level of the spectra to give the negative of the DOS value for the complex, which is called the theoretically generalized-Koopman-theorem-shifted DOS.[53,56] The comparison of simulated DOS with experimental PE spectra (193 nm) of $[Pb_mC_5H_4N]^-$ is shown in Figures 5–8. Here, it should be noticed that when comparing the DOS spectrum with the PE spectra, the important aspect is that the electron binding energy corresponds to each feature but not the relative intensity. The relative intensity also depends on other factors such as the unknown orbital-dependent photodetachment cross-section.

[PbC$_5$H$_4$N]$^-$. The calculation reveals that the structure of the triplet state is more stable than that of the singlet state for $[PbC_5H_4]^-$. The lead atom couples with the pyridyl through the Pb−C bond in a planar manner for both neutral and anionic complexes. The (m, p)-^{3}**1a** PbC_5H_4N are more stable than the o-^{3}**1a**. As listed in Table 1, the calculated EAs of (o, m, p)-^{3}**1a** PbC_5H_4N are 0.89, 1.29, and 1.40 eV, respectively. The experimental result is 1.3 eV. Clearly, the EAs of (m, p)-^{3}**1a** PbC_5H_4N correspond better with the experimental result than that of o-^{3}**1a**. The comparison between the PE spectra of $[PbC_5H_4]^-$ and the theoretically simulated DOS for structures (o, m, p)-^{3}**1a** are presented in Figure 5. It can be seen that none of the calculated spectra matches the experimental data well. Only a combination of all calculated DOSs is able to match the experimental data. Therefore, all the (o, m, p)-^{3}**1a** are suggested to be present in the products. Also, we calculate the EA of $[C_5H_5NPb]^-$ to be 0.52eV, which cannot match the experimental data. Obviously, the product of $[C_5H_5NPb]^-$ can be ruled out safely.

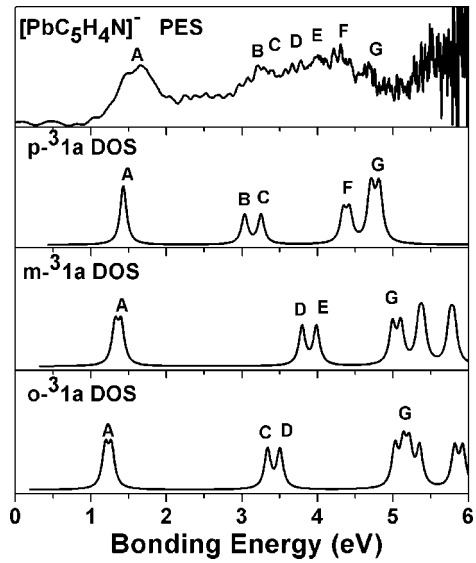

Figure 5. Comparison of PE spectra (193 nm) with theoretical simulated Koopman-theorem-shifted DOS for the optimized ground-state structure of $[PbC_5H_4N]^-$.

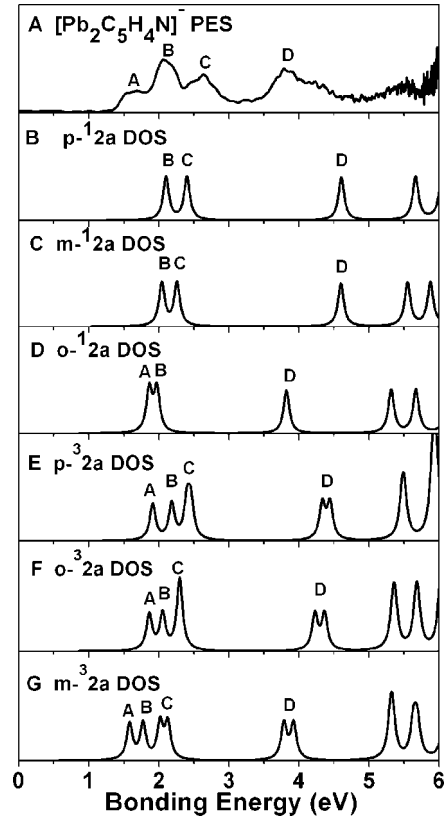

Figure 6. Comparison of PE spectra (193 nm) with theoretical simulated Koopman-theorem-shifted DOS for the optimized ground-state structure of $[Pb_2C_5H_4N]^-$.

[Pb$_2$C$_5$H$_4$]$^-$. The energy difference between singlet state and triplet state for $[Pb_2C_5H_4]^-$ is small, and the (m, p)-^{1,3}**2a** are more stable than the o-^{1,3}**2a**. As listed in Table 2, the calculated EAs of structures (o, m, p)-^{1}**2a** are 1.08, 1.74, and 1.80 eV, respectively. And the calculated EAs of the (o, m, p)-^{3}**2a** are 0.94, 1.56, and 1.94 eV, respectively. The experimental result is 1.48 eV. Obviously, the EAs of (m, p)-^{1,3}**2a** are larger than

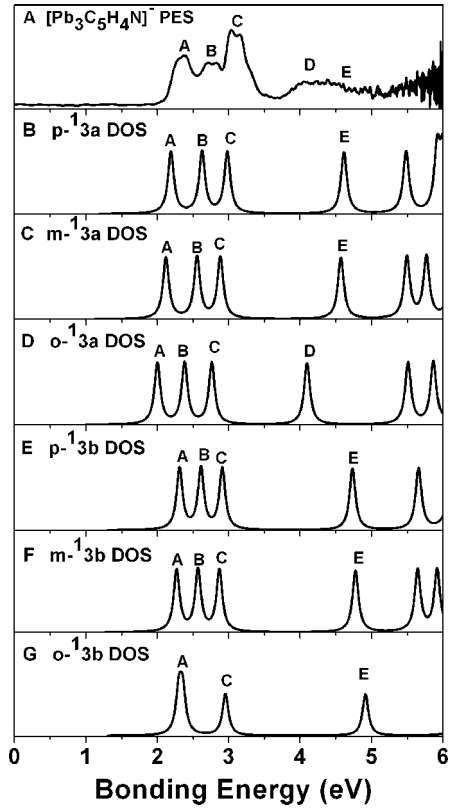

Figure 7. Comparison of PE spectra (193 nm) with theoretical simulated Koopman-theorem-shifted DOS for the optimized ground-state structure of $[Pb_3C_5H_4N]^-$.

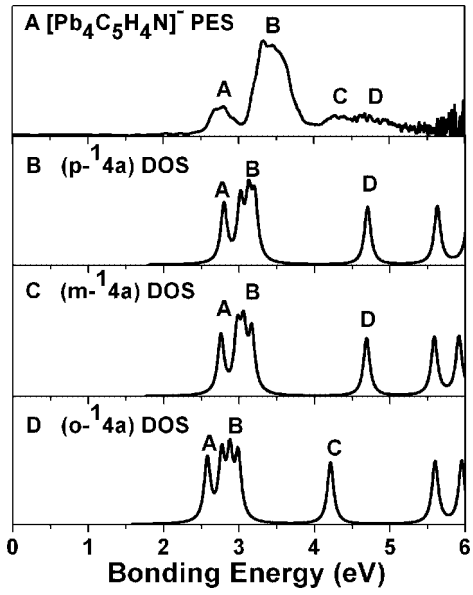

Figure 8. Comparison of PE spectra (193 nm) with theoretical simulated Koopman-theorem-shifted DOS for the optimized ground-state structure of $[Pb_4C_5H_4N]^-$.

the experimental EA and near the value of peak B. Moreover, the calculated VDEs of (m, p)- ^{1}**2a** are 1.88 and 1.85 eV and those of (m, p)- ^{3}**2a** are 1.98 and 1.95 eV, which are also near the peak-B value of 2.0 eV. The VDEs of o-^{1,3}**2a** are 1.65 and 1.71 eV, which corresponded to the peak-A value of 1.7eV. Therefore, we think that the PE spectra is a combination of DOS of all (o, m, p)-^{1,3}**2a** isomers. As shown in Figure 6, the calculated individual DOS of structures (o, m, p)-^{1,3}**2a** match the experimental PE spectra partly, whereas their combination

TABLE 3: Various Structural and Energetic Characteristics for Complexes of $[Pb_3C_5H_4N]^-$

cluster	isomer	R_{Pb-C} (Å)	ΔE (eV)	EA (eV)
$[Pb_3C_5H_4N]^-$	p-^{1}3a	2.38	0	2.06
	p-^{1}3b	2.37	0.16	1.90
	p-^{1}3c	2.28	0.40	1.66
	p-^{1}3d	2.29	0.41	1.66
	p-^{1}3e	2.34	0.51	1.55
	p-^{3}3a	2.420	0.89	1.17
	p-^{3}3b	2.346	0.45	1.61
	p-^{3}3c	2.346	0.77	1.29
	m-^{1}3a	2.388	0.08	1.96
	m-^{1}3b	2.365	0.19	1.87
	m-^{1}3c	2.285	0.46	1.58
	m-^{1}3d	2.291	0.45	1.60
	m-^{1}3e	2.340	0.58	1.46
	m-^{3}3a	2.526	0.86	1.18
	m-^{3}3b	2.343	0.48	1.56
	m-^{3}3c	2.347	0.81	1.23
	o-^{1}3a	2.367	0.20	1.88
	o-^{1}3b	2.361	0.22	1.87
	o-^{1}3c	2.277	0.62	1.47
	o-^{1}3d	2.301	0.66	1.43
	o-^{1}3e	2.335	0.68	1.41
	o-^{3}3b	2.334	0.65	1.24
	o-^{3}3c	2.319	0.95	1.14

DOS match the experimental PE spectra well. Therefore, it is suggested that the complexes of (o, m, p)-^{1,3}**2a** are all present in the products.

[$Pb_3C_5H_4$]$^-$. Calculation reveals that the lowest-energy ground state of $[Pb_3C_5H_4]^-$ is the singlet state. The (m, p)-^{1}**3a** have small energy differences and are more stable than o-^{1}**3a**. The calculated EA values of the structures (o, m, p)**-3a** are 1.89, 1.96, and 2.06 eV, respectively. The experimental value is 2.17eV. The calculated DOS of structures (o, m, p)-^{1}**3a** are shown in Figure 7. It can be seen that the combined DOS of (o, m, p)-^{1}**3a** matches the experiment well. The singlet-state structure **3b** is nearest to that of **3a** in energy. The EAs and DOS of (o, m, p)**-^{1}3b** also correspond to the experimental result. Therefore, it is suggested that the structures (o, m, p)-^{1}(**3a**,**b**), in which the pyridyl couples on the lead atom through a single Pb−C bond, are all present in the product of $^1[Pb_3C_5H_4]^-$.

[$Pb_4C_5H_4$]$^-$. Isomer ^{1}**4a** is the lowest-energy structure. As listed in Table 4, the (m, p)-^{1}**4a** have small energy differences and are more stable than o-^{1}**4a**. The EAs of structures (o, m, p)-**4a** of the singlet state are 2.58, 2.60, and 2.68 eV, respectively. The experimental EA is 2.59 eV. Obviously, the p-^{1}**4a** and m-^{1}**4a** are in better agreement with the experiment than o-^{1}**4a**. The simulated DOS of structures (o, m, p)-**4a** of the singlet state are shown in Figure 8. Also, p-^{1}**4a** and m-^{1}**4a** match the PE spectra better than o-^{1}**4a**. Therefore, (m, p)-^{1}**4a** are the predominant products, and minor o-^{1}**4a** is also present in the $[Pb_4C_5H_4]^-$ products. It should be mentioned that the optimized geometry ^{1}**4a** is also similar to those of Pb_4F and $Pb_4C_6H_5$,[36,37] in which the F atom or phenyl combines on lead clusters by the Pb−F or Pb−C σ bond with a closed-shell electron structure, and the Pb_4 have a rhombus configuration. This provides further evidence that the ^{1}**4a** of $[Pb_4C_5H_4]^-$ is reasonable.

4.4. Analysis of Molecular Orbital Composition. The molecular orbital composition for the anion complex is analyzed, and the calculated MO pictures of $[Pb_mC_5H_4N]^-$ are given in Figure 9. For the ground-state $[PbC_5H_4N]^-$, the HOMO and HOMO-1 are mostly from the $6p_x$ and $6p_y$ of the Pb atom, and they are nonbonding MOs for the Pb−C part. The HOMO-2 is formed by interaction from 6s and $6p_z$ of the Pb atom with 18A′

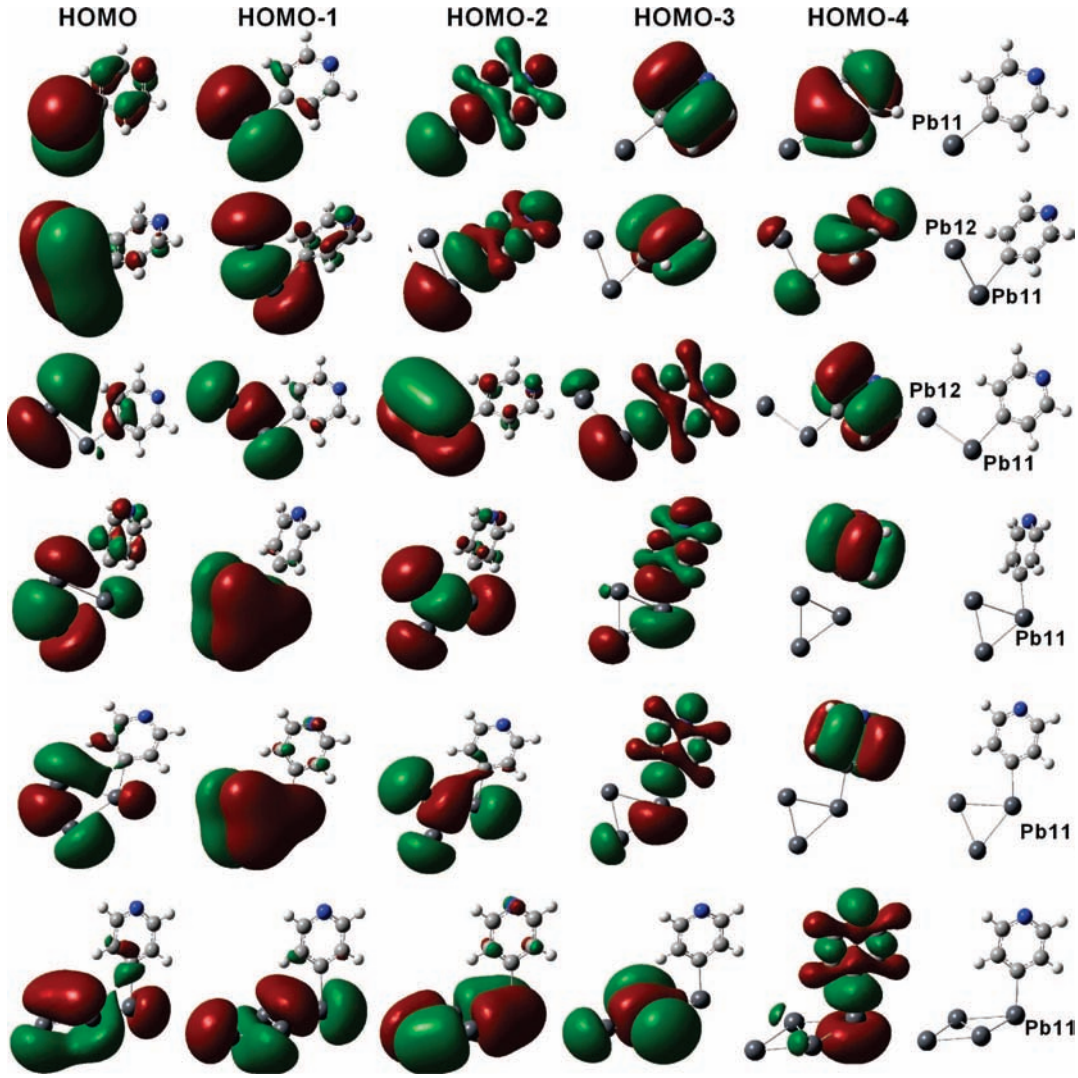

Figure 9. Molecular orbital pictures for para-position structure of ^{3}**1a**, ^{1,3}**2a**, ^{1}(**3a**,**b**), and ^{1}**4a**. The last picture in each row is the coordinate sketch of the cluster complex corresponding to its molecular orbital pictures.

of C_5H_4N, which is a σ MO for the Pb−C part. Following the HOMO-2, the inner MOs of $[PbC_5H_4N]^-$ are only from the C_5H_4N part, which are nonbonding MOs for the Pb−C part. Therefore, the Pb atom and the pyridyl bind together by the σ bond, in which the SP hybridized orbital of the Pb atom interacts with the 18A′ of C_5H_4N (mainly formed with $2p_z$ orbital of the nearest C atom).

There are two possible spin-state structures for $[Pb_2C_5H_4N]^-$. As for ^{1}**2a**, the HOMO is from the $6p_x$ interaction of two Pb atoms, and the HOMO-1 is from the $6p_y$ interaction of two Pb atoms. These two MOs are local π-type and σ-type bonds between two Pb atoms, respectively. The HOMO-2 is formed by interaction from 6s and $6p_z$ of Pb atoms with 18A′ of C_5H_4N, which is a σ MO for the Pb−C part. The inner MOs are similar to the case of $[PbC_5H_4N]^-$, with nonbonding MOs for the Pb−C part. Therefore, the nearest Pb atom and the pyridyl bind together by the σ bond, in which 6s and $6p_z$ orbits of the nearest Pb atom hybridize, and then bond with the $2p_z$ orbital of the nearest C atom. As for the ^{3}**2a**, the HOMO is mostly from the $6p_x$ of the terminal Pb atom, and it is nonbonding MO for the Pb−C part. The HOMO-1 is formed mostly by interaction from the $6p_y$ of two Pb atoms, which is a π-type bond between two Pb atoms and a nonbonding MO for the Pb−C part. The HOMO-2 is formed by interaction from the 6s and $6p_z$ of Pb atoms with 18A′ of C_5H_4N, which is a σ MO for the Pb−C part. The inner MOs are similar to the **2a**, with nonbonding MOs for the Pb−C part. Therefore, the nearest Pb atom and the pyridyl bind together by the σ bond, in which the SP hybridized orbit of the Pb atom bonds with the $2p_z$ orbital of the nearest C atom.

For $[Pb_3C_5H_4N]^-$, the HOMO, HOMO-1, and HOMO-2 are mostly the local MOs between Pb atoms. Only the HOMO-3 is a σ MO for the Pb−C part, and the inner MOs also are nonbonding MOs for the Pb−C part. Therefore, we conclude that in $[Pb_3C_5H_4N]^-$, the Pb_3 cluster connects with the pyridyl by the Pb−C σ bond. Similar cases can be seen for the complex $[Pb_4C_5H_4N]^-$, and there is only one σ MO for the Pb−C part. For all $[Pb_mC_5H_4]^-$ complexes, the number of outer local MOs (meaning the MOs with the higher energy level of the assigned σ MO for the Pb−C part) between Pb atoms is equal to the number of Pb atoms. This result also indicates that the PE spectra features for larger m of $[Pb_mC_5H_4N]^-$ are like those of the PE spectra of Pb_m^-. For each of the $[Pb_mC_5H_4N]^-$ complexes, there exists only one σ MO for the Pb−C part, which can be evidence that pyridyl binds on lead clusters through the Pb−C σ bond. This interaction can also influence the energy level of the outer MOs to result in the electron detachment threshold of $[Pb_mC_5H_4N]^-$ complexes being higher than that of $[Pb_m]^-$. Moreover, it is obvious that the lone-pair electron of nitrogen atom of pyridyl does not take part in the outer local

TABLE 4: Various Structural and Energetic Characteristics for Complexes of [Pb$_4$C$_5$H$_4$N]$^-$

cluster	isomer	R_{Pb-C} (Å)	ΔE eV)	EA(eV)
[Pb$_4$C$_5$H$_4$N]$^-$	p-^{1}4a	2.359	0	2.68
	p-^{1}4b	2.321	0.41	2.58
	p-^{3}4a	2.355	0.85	1.83
	p-^{3}4b	2.348	0.92	2.07
	m-^{1}4a	2.355	0.02	2.64
	m-^{1}4b	2.321	0.45	2.56
	m-^{3}4a	2.352	0.89	1.78
	m-^{3}4b	2.350	0.97	2.04
	o-^{1}4a	2.351	0.19	2.46
	o-^{1}4b	2.311	0.60	2.99
	o-^{3}4a	2.347	1.04	1.97
	o-^{3}4b	2.340	1.10	0.13

MOs, which leads to the similar PE spectra of (p, m, o)-[Pb$_m$C$_5$H$_4$N]$^-$. This also provides the evidence that the PE spectra of [Pb$_m$C$_5$H$_4$N]$^-$ is similar to that of [Pb$_m$C$_6$H$_5$]$^-$ complexes.[36]

Because of the different charge distribution of o, m, p-position of nitrogen atom in pyridine, it is suggested that the different attacking patterns of anion lead cluster to pyridine lead to the different rates of production of (o, m, p)-[Pb$_m$C$_5$H$_4$N]$^-$ as product. The formation mechanism of (o, m, p)-[Pb$_m$C$_5$H$_4$N]$^-$ will be investigated in our future work.

5. Conclusions

Pyridyl−lead complexes [Pb$_m$C$_5$H$_4$N]$^-$ (m = 1−4) are produced from the reactions between pyridine and lead vapor generated by laser ablation on a lead solid sample. A combined experimental and theoretical effort is made to elucidate the bindings, geometries, and electronic structures of these species. The EAs of Pb$_m$−pyridyl (m = 1−4) are obtained from the experimental PE spectra with 308 and 193 nm laser, which are compared with the theoretical calculation including the EAs and the simulated DOS spectra to assign the most probable structure. The following MO analysis is provided to reveal the bonding mode of Pb−C bond in [Pb$_m$C$_5$H$_4$N]$^-$. All of the results indicate that the C$_5$H$_4$N group acts just like an additional lead atom in the clusters and contributes a single electron to bond on the lead fragment through C−Pb σ bond. All the (o, m, p)-[Pb$_m$C$_5$H$_4$N]$^-$ (m = 1−4) are considered to be present in the products. Moreover, the [PbC$_5$H$_4$N]$^-$ is assigned to be a triplet state as the ground state structure, whereas the [Pb$_2$C$_5$H$_4$N]$^-$ is assigned to a the two-state complex including the singlet state and the triplet state. The assigned structures [Pb$_m$C$_5$H$_4$N]$^-$ (m = 3, 4) present a closed-shell electron ground-state structure of singlet state. Clearly, there is an apparent spin-state transition from triplet state toward singlet state for the ground-state structure of [Pb$_m$C$_5$H$_4$N]$^-$ with the increase of lead cluster.

Acknowledgment. This work was supported by NKBRSF (2007CB815202) and NSFC (20573110, 20433080, 20773126). Most calculations have been done at Virtual Laboratory for Computational Chemistry, CNIC, CAS.

Supporting Information Available: This material is available free of charge via the Internet at http://pubs.acs.org.

References and Notes

(1) Xi, M.; Bent, B. E. *Surf. Sci.* **1992**, *278*, 19.
(2) Yang, M. X.; Xi, M.; Yuan, H.; Bent, B. E.; Stevens, P.; White, J. M. *Surf. Sci.* **1995**, *341*, 9.
(3) Syomin, D.; Kim, J.; Koel, B. E.; Ellison, G. B. *J. Phys. Chem. B* **2001**, *105*, 8387.
(4) Sauer, J. *Chem. Rev.* **1989**, *89*, 199.
(5) Bäckvall, J. E.; Bökman, F.; Blomberg, M. R. A. *J. Am. Chem. Soc.* **1992**, *114*, 534.
(6) Dougherty, D. A. *Science* **1996**, *271*, 163.
(7) Szilagyi, R. K.; Frenking, G. *Organometallics* **1997**, *16*, 4807.
(8) Kitagawa, S.; Kitaura, R.; Noro, S. *Angew. Chem., Int. Ed.* **2004**, *43*, 2334.
(9) Loffreda, D. *Angew. Chem., Int. Ed.* **2006**, *45*, 6537.
(10) Zhong, Q. L.; Zhang, B.; Ding, Y. M.; Liu, Y. L.; Rao, G. S.; Wang, G. F.; Ren, B.; Tian, Z. Q. *Acta Phys. Chim. Sin.* **2007**, *23*, 1432.
(11) Vattuone, L.; Gerbi, A.; Rocca, M.; Valbusa, U.; Pirani, F.; Vecchiocattivi, F.; Cappelletti, D. *Angew. Chem., Int. Ed.* **2004**, *43*, 5200.
(12) Veal, J. M.; Rill, R. L. *Biochemistry* **1989**, *28*, 3243.
(13) Sigman, D. S.; Bruice, T. W.; Mazumder, A.; Sutton, C. L. *Acc. Chem. Res.* **1993**, *26*, 98.
(14) Anipsitakis, G. P.; Dionysiou, D. D. *Appl. Catal., B* **2004**, *54*, 155.
(15) Tung, K.; Presley, B. J. *Anal. Chem.* **2002**, *74*, 4716.
(16) Xu, G.; Dong, S. *Anal. Chem.* **2000**, *72*, 5308.
(17) Norkus, E.; Stalnioniene, I.; Crans, C. D. *Heteroat. Chem.* **2003**, *7*, 625.
(18) Cao, P. G.; Gu, R. A.; Ren, B.; Tian, Z. Q. *Chem. Phys. Lett* **2002**, *366*, 440.
(19) Gu, R. A.; Cao, P. G.; Yao, J. L.; Ren, B.; Xie, Y.; Mao, B. W.; Tian, Z. Q. *J. Electroanal. Chem.* **2001**, *505*, 95.
(20) Huang, Q. J.; Lin, X. F.; Yang, Z. L.; Hu, J. W.; Tian, Z. Q. *J. Electroanal. Chem.* **2004**, *563*, 121.
(21) Wu, D. Y.; Duan, S.; Ren, B.; Tian, Z. Q. *J. Raman. Spectrosc.* **2005**, *36*, 533.
(22) Wu, D. Y.; Ren, B.; Jiang, Y. X.; Xu, X.; Tian, Z. Q. *J. Phys. Chem. A* **200**, *106*, 9042.
(23) Wu, D. Y.; Ren, B.; Xu, X.; Liu, G. K.; Yang, Z. L.; Tian, Z. Q. *J. Chem. Phys.* **2003**, *119*, 1701.
(24) Xie, Y.; Wu, D. Y.; Liu, G. K.; Huang, Z. F.; Ren, B.; Yan, J. W.; Tian, Z. Q. *J. Electroanal. Chem* **2003**, *554*, 417.
(25) Rodgers, M. T.; Stanley, J. R.; Amunugama, R. *J. Am. Chem. Soc.* **2000**, *122*, 10969.
(26) Yang, Y. S.; Hsu, W. Y.; Lee, H. F.; Huang, Y. C.; Yeh, C.S.; Hu, C.H. *J. Phys. Chem. A.* **1999**, *103*, 11287.
(27) Hsu, H. C.; Lin, F. W.; Lai, C. C.; Su, P. H.; Yeh, C. S. *New J. Chem.* **2002**, *26*, 481.
(28) Venkatachalapathy, R.; Davila, G. P.; Prakash, J. *Electrochem. Commun.* **1999**, *1*, 614.
(29) Halligudi, S. B.; Kala Raj, N. K.; Rajani, R.; Unni, I. R.; Gopinathan, S. *Appl. Catal., A* **2000**, *204*, L1.
(30) Tang, I. N.; Castleman, A. W. *J. Chem. Phys.* **1972**, *57*, 3638.
(31) Guo, B. C.; Purnell, J. W.; Castleman, A. W., Jr *Chem. Phys. Lett.* **1990**, *168*, 155.
(32) Barran, P. E.; Mikhailov, V.; Stace, A. J. *J. Phys. Chem. A* **1999**, *103*, 8792.
(33) Xing, X. P.; Tian, Z. X.; Liu, H. T.; Tang, Z. C. *J. Phys. Chem. A* **2003**, *107*, 8484.
(34) Tian, Z. X.; Xing, X. P.; Tang, Z. C. *Rapid Commun. Mass Spectrom.* **2002**, *16*, 1515.
(35) Tian, Z. X.; Xing, X. P.; Tang, Z. C. *Rapid Commun. Mass Spectrom.* **2003**, *17*, 17.
(36) Liu, H. T.; Xing, X. P.; Sun, S. T.; Gao, Z.; Tang, Z. C. *J. Phys. Chem. A* **2006**, *110*, 8688.
(37) Negishi, Y.; Kawamata, H.; Nakajima, A.; Kaya, K. *J. Electron Spectrosc. Relat. Phenom.* **2000**, *106*, 117.
(38) Ganteför, G.; Gausa, M.; Meiwes-Broer, K. H.; Lutz, H. O. *Z. Phys. D* **1989**, *12*, 405.
(39) Luder, C.; Meiwes-Broer, K. H. *Chem. Phys. Lett.* **1998**, *294*, 391.
(40) Ho, J.; Polak, M.; Lineberger, W. C. *J. Chem. Phys.* **1992**, *96*, 144.
(41) Xing, X. P.; Tian, Z. X.; Liu, P.; Gao, Z.; Zhu, Q.; Tang, Z. C. *Chin. J. Chem. Phys.* **2004**, *17*, 321.
(42) Frisch, M. J.; Trucks, G. W.; Schlegel, H. B.; Scuseria, G. E.; Robb, M. A.; Cheeseman, J. R.; Montgomery, J. A., Jr.; Vreven, T.; Kudin, K. N.; Burant, J. C.; Millam, J. M.; Iyengar, S. S.; Tomasi, J.; Barone, V.; Mennucci, B.; Cossi, M.; Scalmani, G.; Rega, N.; Petersson, G. A.; Nakatsuji, H.; Hada, M.; Ehara, M.; Toyota, K.; Fukuda, R.; Hasegawa, J.; Ishida, M.; Nakajima, T.; Honda, Y.; Kitao, O.; Nakai, H.; Klene, M.; Li, X.; Knox, J. E.; Hratchian, H. P.; Cross, J. B.; Bakken, V.; Adamo, C.; Jaramillo, J.; Gomperts, R.; Stratmann, R. E.; Yazyev, O.; Austin, A. J.; Cammi, R.; Pomelli, C.; Ochterski, J. W.; Ayala, P. Y.; Morokuma, K.; Voth, G. A.; Salvador, P.; Dannenberg, J. J.; Zakrzewski, V. G.; Dapprich, S.; Daniels, A. D.; Strain, M. C.; Farkas, O.; Malick, D. K.; Rabuck, A. D.; Raghavachari, K.; Foresman, J. B.; Ortiz, J. V.; Cui, Q.; Baboul, A. G.; Clifford, S.; Cioslowski, J.; Stefanov, B. B.; Liu, G.; Liashenko, A.; Piskorz, P.; Komaromi, I.; Martin, R. L.; Fox, D. J.; Keith, T.; Al-Laham, M. A.; Peng, C. Y.; Nanayakkara, A.; Challacombe, M.; Gill, P. M. W.; Johnson,

B.; Chen, W.; Wong, M. W.; Gonzalez, C.; Pople, J. A. *Gaussian 03*, revision C.02; Gaussian, Inc.: Wallingford, CT, 2004.

(43) (a) Lee, C.; Yang, W.; Parr, R. G. *Phys. Rev.* **1988**, *B37*, 785. (b) Becke, A. D. *J. Chem. Phys.* **1993**, *98*, 1372–5648. (c) Becke, A. D. *Phys. Rev.* **1988**, *A38*, 3098.

(44) (a) Wadt, W. R.; Hay, P. J. *J. Chem. Phys.* **1985**, *82*, 284. (b) Hay, P. J.; Wadt, W. R. *J. Chem. Phys.* **1985**, *82*, 299. (c) Check, C. E.; Faust, T. O.; Bailey, J. M.; Wright, B. J.; Gilbert, T. M.; Sunderlin, L. S. *J. Phys. Chem. A* **2001**, *105*, 8111.

(45) Tsai, M. L.; Su, M. D. *J. Phys. Chem. A* **2006**, *110*, 6216.

(46) Whittleton, S. R.; Boyd, R. J.; Grindley, T. B. *J. Phys. Chem. A* **2006**, *110*, 5893.

(47) Su, M. D. *Inorg. Chem.* **2004**, *43*, 4846.

(48) Goldfuss, B.; Schleyer, P. v. R. *Organometallics* **1997**, *16*, 1543.

(49) Su, M. D. *J. Phys. Chem. A* **2002**, *106*, 9563.

(50) Chen, D. L.; Tian, W. Q.; Feng, J. K.; Sun, C. C. *J. Phys. Chem. A* **2007**, *111*, 8277.

(51) Metz, B.; Stoll, H.; Dolg, M. *J. Chem. Phys.* **2000**, *113*, 2563.

(52) Peterson, K. A. *J. Chem. Phys.* **2003**, *119*, 11099.

(53) Ganteför, G.; Gausa, M.; Meiwes-Broer, K. H.; Lutz, H. O. *Z. Phys. D* **1989**, *12*, 405.

(54) Ho, J.; Polak, M.; Lineberger, W. C. *J. Chem. Phys.* **1992**, *96*, 144.

(55) Jonathan, C. R.; Gregory, S. T.; Henry, F. S.; Sreela, N.; Ellison, G. B. *Chem. Rev.* **2002**, *102*, 231.

(56) Wang, B. L.; Zhao, J. J.; Chen, X. S.; Shi, D. N.; Wang, G. H. *Phys. Rev. A* **2005**, *71*, 033201.

(57) Li, J.; Li, X.; Zhai, H. J.; Wang, L. S. *Science* **2003**, *299*, 864.

(58) Issendorff, B. V. *Phys. Rev. Lett.* **2004**, *93*, 93401.

(59) Häkkinen, H.; Moseler, M.; Landman, U. *Phys. Rev. Lett.* **2002**, *89*, 33401.

(60) Häkkinen, H.; Yoon, B.; Landman, U.; Li, X.; Zhai, H. J.; Wang, L. S. *J. Phys. Chem. A* **2003**, *107*, 6168.

(61) Li, X.; Kiran, B.; Li, J.; Zhai, H. J.; Wang, L. S. *Angew. Chem., Int. Ed.* **2002**, *41*, 4786.

(62) Wang, L. S.; Wang, X. B.; Wu, H.; Cheng, H. *J. Am. Chem. Soc.* **1998**, *120*, 6556.

JP711459X